

AUTOMATIC READOUT OF CONTRAST-DETAIL CURVE USED IN DIGITAL MAMMOGRAPHY USING MORPHOLOGICAL GRANULOMETRY

Angel R. Contreras^a and Omaira Rodríguez^b

^a*Instituto Nacional de Bioingeniería, Universidad Central de Venezuela, Ciudad Universitaria, Av. Los Estadios, Los Chaguaramos, Caracas-Venezuela* angel.contreras@inabio.edu.ve
<http://www.inabio.edu.ve>

^b*Centro de Computación Gráfica, Universidad Central de Venezuela, Facultad de Ciencias, Av. Los Ilustres, Los Chaguaramos, Caracas-Venezuela* omaira.rodriguez@ciens.ucv.ve <http://ccg.ciens.ucv.ve/>

Keywords: Digital Mammography, CDMAM, Mathematical Morphology, Granulometry.

Abstract. Mammography is one of the most effective methods used today for early breast cancer detection. Mammography equipment, is able to take breast radiographies, and is specially designed for it. Quality Control and Quality Assurance, provides a guarantee for the best possible image quality with an acceptable radiation dose. Threshold contrast visibility is one of several tests used in quality control, with international recognition for the acceptance of the system. This test is possible thanks to image processing of the CDMAM (Contrast-Detail Mammography) Phantom.

This paper presents a new algorithm, called MIQ (MammoIQ), for evaluating the CDMAM phantom used in digital mammography. The method consists on evaluating each cell using Mathematical Morphology and digital image processing techniques to determine the eccentric disks. Granulometry concepts are introduced for the CDMAM phantom, pattern spectrum and size distribution. The results are compared with the CDCOM software and a human observer, through the Image Quality Factor (IQF) parameter and Contrast-Detail Curve. The combined results, allow to compare different curves from several images, and to compare the performance of different systems.

Twenty-eight (28) images are analyzed. They are acquired from three different systems, and gathered into three different groups (Systems 1, 2 and 3) according to the system where they were acquired. The calculated metrics used are Contrast-Detail Curve, Size Distribution, Pattern Spectrum, and Image Quality Factor (IQF). System 2 presents a better contrast-to-detail ratio with respect to the other systems. The results obtained with the algorithm MIQ present a greater similarity to the results obtained by human observers. The presented algorithm provides non-ambiguous and fast results for expert and non-expert evaluators.

1 INTRODUCTION

Breast cancer is one of the main causes of death in women around the world. Government and non governmental organizations, research centers, companies, and others have invested a lot of effort, time and money, to provide early detection for this disease. Magnetic resonance, ultrasound, computed tomography and mammography are the most common techniques for detection and diagnosis of breast cancer (Feig et al., 2004). Mammography is the gold standard, because of its high resolution and relatively low costs.

High resolution and good image quality can be achieved through methods and tests called Quality Assurance and Quality Control, in which the system must be tested. To guarantee image quality, manufacturers and research centers have issued quality control manuals to assure the best image quality with as low as possible radiation doses (Feig et al., 2004; Siemens A. G., 2008; Cerezo, 2006).

Threshold contrast visibility is one of several tests used in digital mammography (Perry et al., 2006). This test consists in determining the contrast threshold associated with circular objects (disks). Diameter disks are between $0,06mm$ and $2,0mm$, and thickness disks are between $0,03\mu m$ and $2,00\mu m$. An evaluator can spend around 75 to 90 minutes to perform the test for digital systems or analog systems with CR (Computed Radiography) (Chevalier et al., 2007). Moreover, is needed an expert observer with training in this field, to obtain reliable results.

A CDMAM phantom is used to perform the test, it has a rectangular shape and 205 cells containing disks of 99.99% pure gold.

The phantom is placed between two pieces of plexiglass $20mm$ each, in order to get $45mm$ of thickness, that is equivalent to a breast with $60mm$ thickness. Later, an exposure in Automatic Exposure Control (AEC) is take, selecting the normal clinical settings used in the system. Then, the raw image is analyzed, that means without processing. The procedure should be repeated shifting the phantom slightly, with the purpose of varying the relative position of details with respect to detector elements. The observer uses a template, which should indicate the right position of the visualized eccentric disks. The next step is comparing the original pattern with the eccentric disk detected, for penalizing each cell using nearest neighbor correction, and then determining threshold contrast visibility (Karssemeijer and Thijssen, 2004; Feig et al., 2004).

Since this procedure is time consuming, tedious, and results depend on the errors and experience of the observer, we propose an algorithm that provides an automatic tool for the evaluation and analysis of CDMAM.

2 METHODOLOGY

The methodology is based on mathematical morphology methods, in order to automatically detect the grid of the phantom. Every cell is labeled, isolated and processed individually for determining its eccentric disk. After the eccentric disks have been determined, the detected position is compared against an evaluation form containing the correct position of the eccentric disk. The algorithm reads the eccentricity matrix and corrects the Contrast-Detail Curve using the nearest neighbor correction. Once every disk is reconstructed, granulometry is applied.

2.1 Definition of Structuring Elements

There are plenty of sizes and shapes of Structuring Elements (SEs). The size and shape for the Structuring Element will be selected according to the object to be analyzed. However, there are two SEs with special importance, SE_{45} and SE_{-45} . Both of them have straight line shape, but with orientation 45° and -45° degrees respectively. The size of each SE in pixels

N_{px} , is equal to the size of one side of a cell in the phantom S_O (see Fig. 1) multiplied by the magnification M and divided by the pixel physical size IPS . Eq.1 shows the size of each SE in pixels.

$$N_{px} = \frac{M \cdot S_O}{IPS} \quad (1)$$

From SE_{45} and SE_{-45} it is possible to construct SE , it has size and shape equal to a cell of CDMAM. Fig. 1 shows the main SEs used in this work.

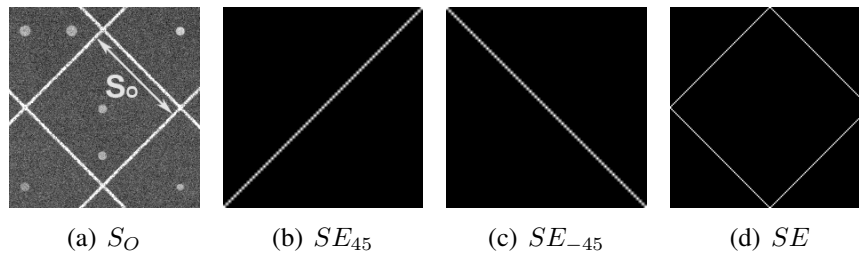


Figure 1: (a) Object size used to construct SE. (b) SE with straight line shape and 45 degree. (c) SE with straight line shape and -45 degree. (d) SE with size and shape equal to a cell of CDMAM. The sizes of SEs are determined through the magnification and the pixel physical size.

2.2 Detection Grid

The top-hat transformation is used for shadow correction on the grid. Shadow correction is useful to compensate the Heel effect on the image (Curry et al., 1990; Karssemeijer and Thijssen, 1996). Two morphological openings are made using SE_{45} and SE_{-45} to enhance straight lines in the grid. Fig. 2 shows the result of this operation, I is the original image, I_0 is the original image after the top-hat transformation, I_{45} is the original image after a complete opening with SE_{45} , and similarly I_{-45} is the original image after a complete opening with SE_{-45} .

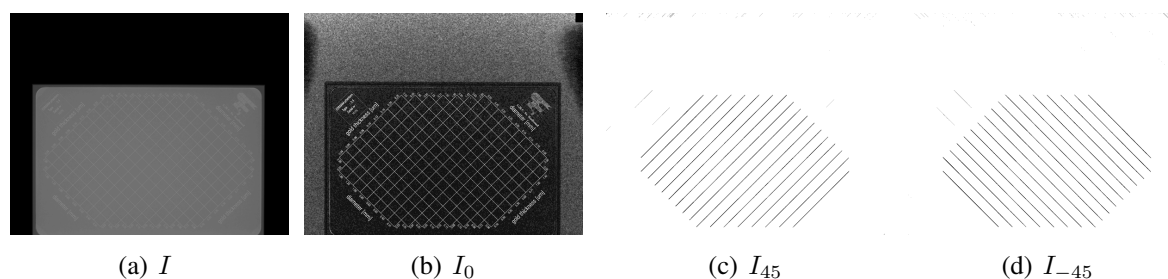


Figure 2: (a) Original image of CDMAM. (b) Shadow correction after applying the top-hat transformation. (c) Image after a complete opening with SE_{45} . (d) Image after a complete opening with SE_{-45} . Images (c) and (d) are shown in negative for a better perception.

I_{45} and I_{-45} are thresholded through Eq. 2 and Eq. 3 respectively, where k has a constant value of 0.1. Fig. 3 shows I_a and I_b results of thresholding. Finally, adding (union of sets) I_a

and I_b , produces I_c (Eq. 4), which contains the grid (see Fig. 3(c)).

$$I_a = \begin{cases} 1, & \text{if } I_{45} > \min(I_{45}) + k(\max(I_{45}) - \min(I_{45})), \\ 0, & \text{otherwise.} \end{cases} \quad (2)$$

$$I_b = \begin{cases} 1, & \text{if } I_{-45} > \min(I_{-45}) + k(\max(I_{-45}) - \min(I_{-45})), \\ 0, & \text{otherwise.} \end{cases} \quad (3)$$

$$I_c = I_a \cup I_b \quad (4)$$

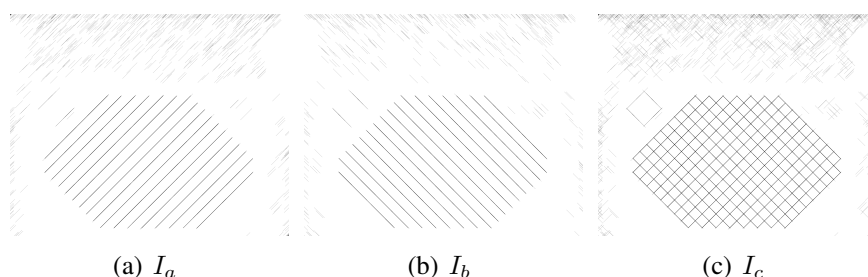


Figure 3: (a) I_a . I_{45} thresholded. (b) I_b . I_{-45} thresholded. (c) I_c . Unions of sets, $I_a \cup I_b$. Images are shown in negative for a better perception.

Several artifacts are presented on image I_c , to solve this problem it is necessary to use an Alternating Sequential Filter (ASF), defined as an opening followed by a closing (Eq. 5) (Contreras and Rodríguez, 2010), where B_1 represents a SE with size and shape equal to a cell, and B_2 represents a square-shaped SE with a size of six pixels.

$$AF_{B_1, B_2} = (A \circ B_1) \bullet B_2 \quad (5)$$

Many of the artifacts are eliminated, however, there are still remains some artifacts on the image. Using 8-adjacency (Gonzalez and Woods, 2008) on I_1 we get I_2 labeled. The histogram of image I_2 is determined $H(I_2)$, and the mode is calculated $mode(H(I_2))$. The mode is the value that occurs the most frequently in a data set, and it also represents the maximum number of pixels labeled. A grid without artifacts is shown in Fig. 4(b) and is called I_m .

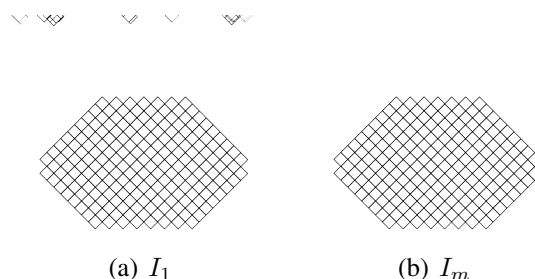


Figure 4: (a) I_1 , many of the artifacts are eliminated. (b) I_m , grid without artifacts. Images shows in negative.

2.3 ROI's Edges

External edges of the grid are located. Through binary images of top border I_{b_t} , bottom border I_{b_b} , left border I_{b_l} and right border I_{b_r} , we calculated the external edges $I_{b_{ex}}$ using the

AND operator. Intersecting Ib_{ex} and I_m we obtain I_{m2} (Eq. 6) as shown in Fig. 5.

$$I_{m2} = Ib_{ex} \cap I_m \quad (6)$$

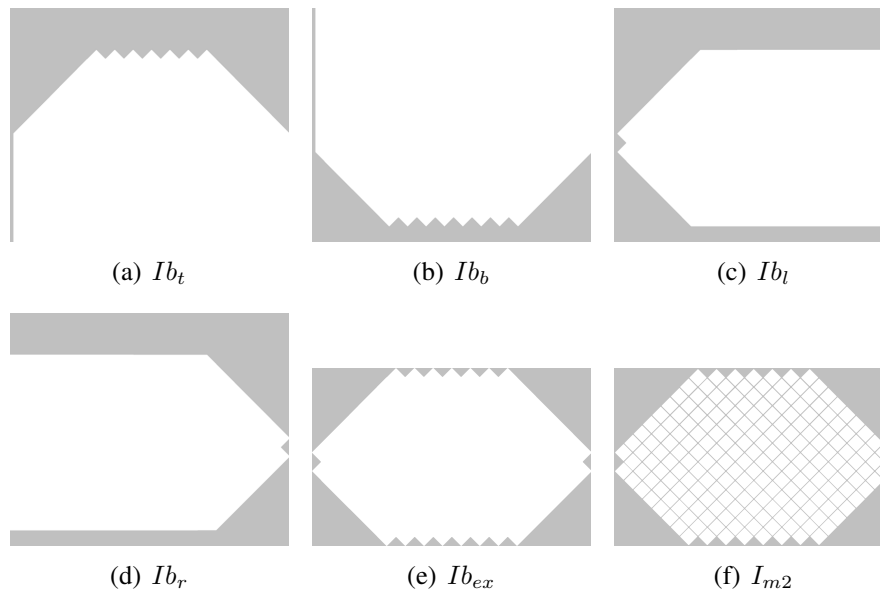


Figure 5: Phantom edges. (a) Top border. (b) Bottom border. (c) Left border. (d) Right border. (e) Intersection of external borders (a), (b), (c) and (d). (f) Cell mask I_{m2} . Intersection of I_m and Ib_{ex} .

2.4 Cells Separation

Every cell must be analyzed individually. Using 8-adjacency, 205 cells in the phantom are labeled from top-left to bottom-right. Cell labeling is required for separating each cell, and for future comparison of results with the evaluation form indicating the right position of eccentric disks.

2.5 Cells Analysis

Cells analysis is done to determine the correct position of eccentric disk. Eccentric disk could be located in four positions: top, left, right, and bottom; they take the values of 1, 2, 4 and 5 respectively. A value of 3 represents the central disk.

Using the evaluation form, it is possible to define the eccentricity matrix. Table 1 shows the eccentricity matrix obtained from the evaluation form (Karssemeijer and Thijssen, 2004).

Every cell is filtered using a Gaussian filter with $\sigma = 0.9$ in order to reduce high-frequency noise. This kind of filter reduces sharpness on borders, to solve this a Kuwahara filter is applied (Preim and Bertz, 2007). A Kuwahara filter preserves border and reduces noise on an image. The Kuwahara kernel is divided into four regions ($i=1,2,3,4$). The output value of the central pixel in the kernel is then set to the mean value m_i of the region R_i which has the smallest variance σ_i^2 . To enhance disk signal, the cell is processed using opening, which allows maximizing regions of interest.

A new mask is defined I_{m4} (see Fig. 6(e)) to detect eccentric disk in the most probably position of the cell. The maximum value is compared in each region, and the region with the greater maximum value is selected. All positions are saved to construct the eccentricity matrix.

D\T	0,03	0,04	0,05	0,06	0,08	0,10	0,13	0,16	0,20	0,25	0,36	0,50	0,71	1,00	1,42	2,00
2,00	-1	5	4	1	2	5	4	1	4	5	-1	-1	-1	-1	-1	-1
1,60	1	1	4	5	4	5	5	1	4	1	2	-1	-1	-1	-1	-1
1,25	1	5	1	1	2	2	1	2	5	5	2	4	-1	-1	-1	-1
1,00	4	2	5	2	5	4	1	5	4	5	1	2	4	-1	-1	-1
0,80	1	1	5	1	4	1	2	4	2	4	4	5	5	1	-1	-1
0,63	2	4	1	2	4	1	2	1	5	2	1	4	4	2	1	-1
0,50	1	2	4	2	2	4	1	5	4	4	5	1	5	1	2	4
0,40	4	1	1	4	5	5	2	1	2	2	5	1	4	1	2	1
0,31	5	5	1	2	1	2	4	4	5	4	2	5	4	5	1	4
0,25	-1	4	2	4	1	5	5	1	1	2	5	5	2	2	1	1
0,20	-1	-1	1	5	2	4	2	5	4	4	5	2	5	5	2	2
0,16	-1	-1	-1	2	1	2	4	4	2	2	4	2	4	1	5	1
0,13	-1	-1	-1	-1	4	2	2	5	2	4	5	1	4	2	4	1
0,10	-1	-1	-1	-1	-1	4	1	4	5	4	5	2	5	2	5	2
0,08	-1	-1	-1	-1	-1	-1	5	4	5	5	1	1	2	5	5	4
0,06	-1	-1	-1	-1	-1	-1	-1	2	4	4	2	4	4	5	2	-1

Table 1: The eccentricity matrix. It is possible to appreciate the numerical position of every disk on the cell. For example: a diameter of $0,50mm$ and thickness of $0,10\mu m$, takes a value of 4, meaning its position is at the right of the central disk. Cells indicating a value of -1 are not present in the CDMAM.

Disk edges are detected using Roberts operator, based on gradient functions. Maximum levels borders are determined, and thresholded for reconstructing disk as shown in the next section. Fig. 6 shows an overview of cell analysis.

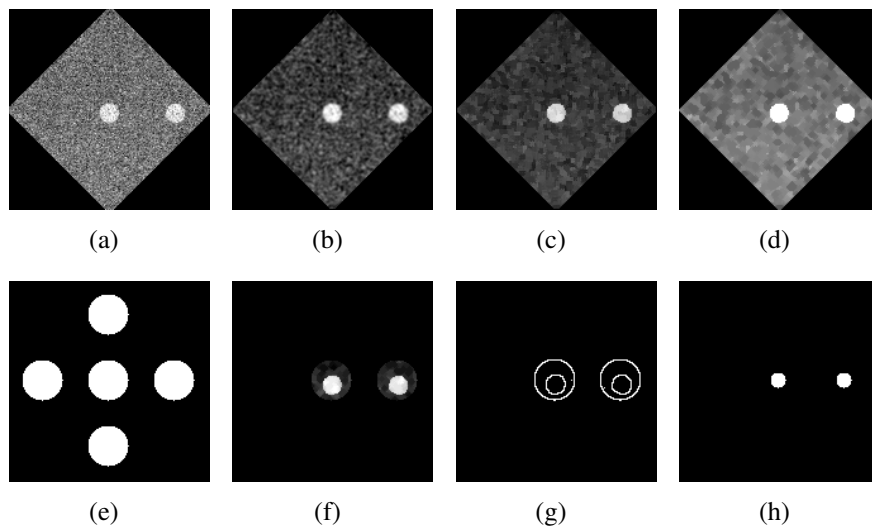


Figure 6: (a) Original cell without processing. (b) Cell after applying the Gaussian Filter. (c) Cell after Kuwahara Filter is applied. (d) Cell after a complete opening is applied with SE square-shape and a size of 2 pixels. (e) Mask I_{m4} . (f) Cell after the maximum is detected. (g) Cell after Roberts operator is applied. (h) Disk reconstruction.

2.6 Disk reconstruction

Disk reconstruction takes eight directions from the center to the borders on the disk. North, north-east, east, south-east, south, south-west, west, north-west radius are calculated (see Fig. 7). r_c represents the average on central disk, and r_e is the average on eccentric disk. Finally, \bar{r} is the maximum average between r_c and r_e .

2.7 Contrast-Detail Curve

The Contrast-Detail Curve is determined for comparing the eccentricity matrix and evaluation form. The results matrix shows which disks were well detected. Notations are similar to

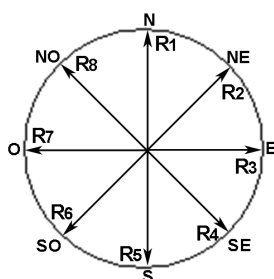


Figure 7: Radius used for reconstructing disk. This procedure is done on eccentric disk and central disk through border detection.

that used by Visser and Karssemeijer (2008).

The curve is determined by thresholding gold thickness for each diameter. The thickness value in a row is given by the first eccentric disk detected correctly in that row. In order to smooth the curve and eliminate isolated cell values, it is necessary to apply nearest neighbor correction. Table 2 shows an example of result matrix after applying the nearest neighbor correction. Usually, The Contrast-Detail Curve is expressed in functions of threshold radiation contrast (%C) as is shown in Karssemeijer and Thijssen (2004). Later, image quality factor (IQF) is calculated for the curve (Verbrugge, 2007). IQF is an image quality quantifier and is denoted as follows

$$IQF = \sum_{i=1}^{16} C_{i,min} \cdot D_i \tag{7}$$

where $C_{i,min}$ is the minimum threshold corresponding to a diameter of D_i .

D\T	0,03	0,04	0,05	0,06	0,08	0,10	0,13	0,16	0,20	0,25	0,36	0,50	0,71	1,00	1,42	2,00
2,00	-1	2	2	1	1	1	1	1	1	1	-1	-1	-1	-1	-1	-1
1,60	2	2	1	1	1	1	1	1	1	1	1	-1	-1	-1	-1	-1
1,25	2	2	1	2	1	1	1	1	1	1	1	1	-1	-1	-1	-1
1,00	2	1	2	2	1	1	1	1	1	1	1	1	1	-1	-1	-1
0,80	2	2	2	2	1	1	1	1	1	1	1	1	1	1	-1	-1
0,63	2	2	2	2	1	1	1	1	1	1	1	1	1	1	1	-1
0,50	2	2	2	1	1	1	1	1	1	1	1	1	1	1	1	1
0,40	2	2	2	2	1	1	1	1	1	1	1	1	1	1	1	1
0,31	1	2	2	2	2	1	2	1	1	1	1	1	1	1	1	1
0,25	-1	2	2	2	2	2	2	2	1	1	1	1	1	1	1	1
0,20	-1	-1	2	2	2	2	2	2	1	1	1	1	1	1	1	1
0,16	-1	-1	-1	2	2	2	2	2	1	1	1	1	1	1	1	1
0,13	-1	-1	-1	-1	2	2	2	2	1	1	1	1	2	1	1	1
0,10	-1	-1	-1	-1	-1	2	2	2	2	2	2	2	1	1	1	1
0,08	-1	-1	-1	-1	-1	-1	2	2	2	2	2	1	1	1	1	2
0,06	-1	-1	-1	-1	-1	-1	-1	2	2	2	2	1	1	1	1	-1

Table 2: An example of the results matrix after applying the nearest neighbor correction. Value 1 indicates the eccentric disk was detected correctly, value 2 wrong detection and value -1 indicates the cell is not present on CDMAM.

2.8 Granulometry

In general terms, granulometry refers to the measurement and classification of particles, grains and rocks in the earth. In digital image processing is an approach to compute a size distribution of grains in binary images, employing a sequence of morphological opening operations (Shih, 2009). There are two main curves used in granulometry: size distribution $D_A(i)$ and pattern spectrum $PS_A(i)$. These curves are calculated theoretically through equations Eq. 8

and Eq. 9 respectively.

$$D_A(i) = \sum_{k=1}^i \pi \left(\frac{d(k)}{2} \right)^2 N_D(k) \quad (8)$$

$$PS_A(i) = \pi \left(\frac{d(i)}{2} \right)^2 N_D(i) \quad (9)$$

where i represents a row in CDMAM, d is the corresponding diameter, and N_D is the number of disks on row i .

3 RESULTS

Twenty-eight (28) images were analyzed in total. They were acquired from three different systems (Table 3) and gathered into three different groups according to the system where they were acquired. Metrics used are Contrast-Detail Curve, Size Distribution, Pattern Spectrum, and Image Quality Factor (IQF). For the images in each system and for each metrics, an average image is computed using our algorithm (MIQ) and compared with CDCOM. For the third system we included the results obtained from human observers (ObsH) of *National Expert and Training Centre for Breast Cancer Screening* (Karssemeijer and Thijssen, 2004). A lower value of Contrast-Detail Curve means a lower IQF that represents a better contrast-to-detail ratio. As shown in Fig. 8(a) to Fig. 8(c), all values of the Contrast-Detail Curves for the three systems are below the achievable values established by EUREF.

Size Distribution (see Fig. 8(d) to Fig. 8(f)) and Pattern Spectrum (see Fig. 8(g) to Fig. 8(i)) are compared against theoretical values. IQF was calculated from results obtained with the algorithm presented (MIQ) in this research: system 1 presents an IQF(1) = 0,7380, system 2 IQF(2) = 0,6650 and system 3 IQF(3) = 0,8341. Similarly, IQF was calculated with the results obtained with the CDCOM: system 1 presents an IQF(1) = 0,5854, system 2 IQF(2) = 0,5526 and system 3 IQF(3) = 0,5883. In both groups of results system 2 presents the lowest IQF values.

Eq.	Model	Manufacturer	Image Size	del	Technology	Software Version
1	MAMMOMAT Inspiration	Siemens A.G.	2800 × 3518	85 μm	Selenium Flat-Panel	VB20B
2	MAMMOMAT Novation ^{DR}	Siemens A.G.	3328 × 4048	70 μm	Selenium Flat-Panel	VA20C
3	Senograph 2000D	GE Healthcare®	1914 × 2294	94 μm	Phosphor Flat-Panel	ADS 17.2.3

Table 3: Summary of some technical features of interest in systems where the analyzed images were acquired. In this table are shown: system (Eq.), model, manufacturer, image size in pixels, detector element size (del), detector technology and software version.

4 CONCLUSIONS AND FUTURE WORK

The new algorithm (MIQ) presents an alternative tool for evaluating CDMAM phantoms, used for expert and non-expert observers, avoiding ambiguous results for the images. This algorithm is mainly based on mathematical morphology. System 2 has obtained the lowest IQF, which indicates a better contrast-to-detail ratio with respect to the other 2 systems, because of its lower IQF for both groups of results obtained from MIQ and CDCOM. Even though, CDCOM presents lower values of the Contrast-Detail Curve, the MIQ algorithm presents a better approximation for human observers in system 3. System 1 presents a better size distribution and pattern spectrum in reference to theoretical values.

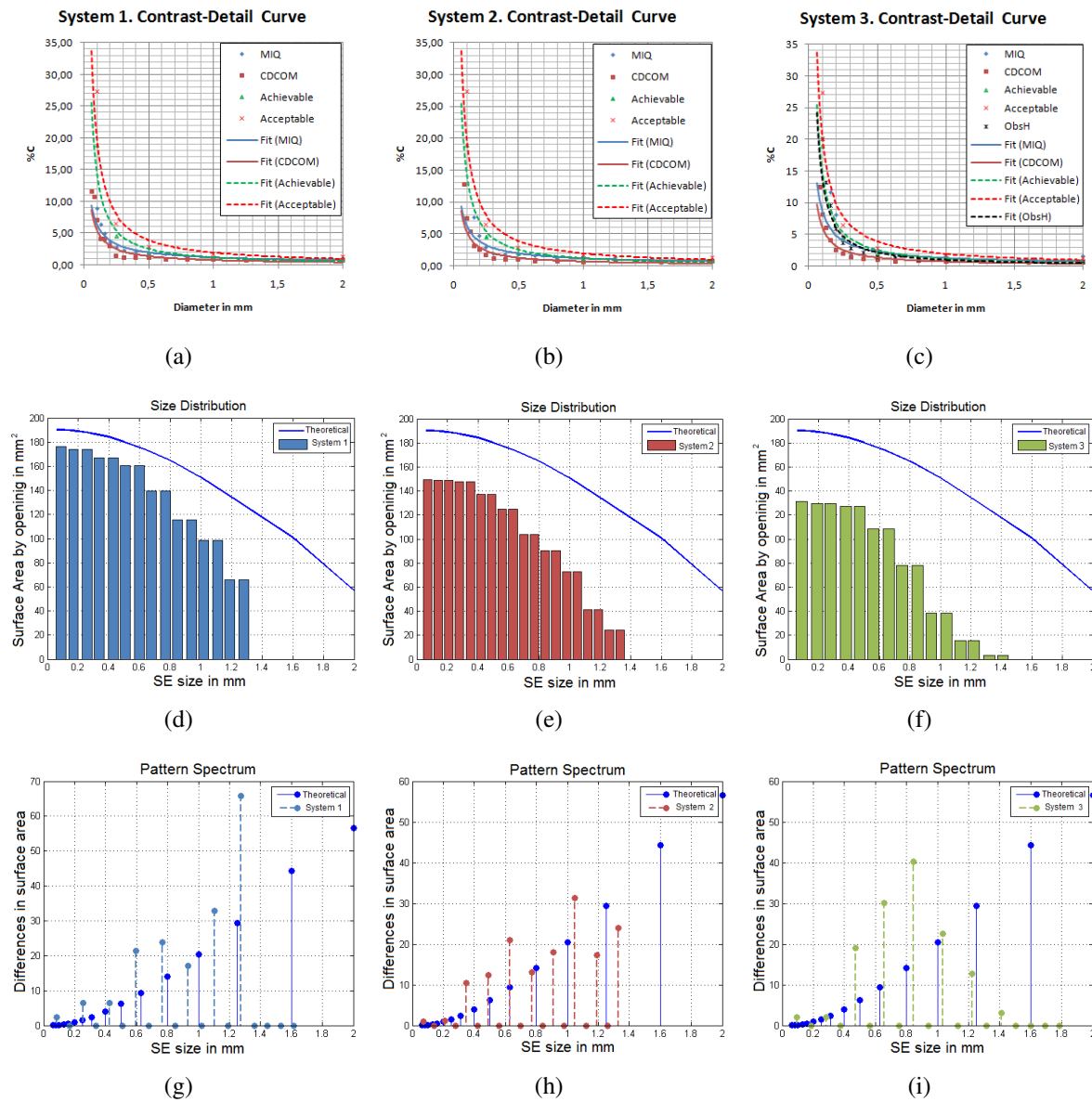


Figure 8: *Contrast-Detail Curve* obtained from algorithm MIQ compared against CDCOM results, achievable and acceptable values for system 1 (a), system 2 (b), and system 3 (c). *Size Distribution* obtained from algorithm MIQ compared against theoretical values for system 1 (d), system 2 (e) and system 3 (f). *Pattern Spectrum* obtained from algorithm MIQ compared against theoretical values for system 1 (g), system 2 (h) and system 3 (i). All curves are fitted.

As future work, we will improve segmentation, edge detection, and disk reconstruction algorithms. As well as provide images for system 1 and 2 evaluated by human observers, in order to compare with results obtained from MIQ algorithm.

5 ACKNOWLEDGMENTS

The authors want to thank to Alexander Urdaneta and Sandro Di Gennaro, from Siemens Healthcare, for their cooperation and provision of images to make possible the development of this work.

REFERENCES

- Cerezo U. Principios de Mamografía, 2006. Siemens, S.A.
- Chevalier M., Morán P., Morant J.J., and Torres R. *Protocolo de control de calidad de los sistemas digitales mamográficos*, 2007.
- Contreras A. and Rodríguez O. Determinación Automática de la Curva Contraste-Detalle en Mamografía Digital empleando Granulometría Morfológica. In *Modelos Computacionales en Ingeniería: Desarrollos Novedosos y Aplicaciones*, pages TC50–TC54. 2010.
- Curry T.S., Dowdey J.E., and Murry R.C. *Christensen's Physics of Diagnostic Radiology*. Williams & Wilkins, Rose Tree Corporate Center, Building II 1400 North Providence Road, Suite 5025 Media, PA 19063-2043 USA, 4ta. edition, 1990.
- Feig S.A., Haus A.G., Hendrick R.E., Howe G.R., McCrohan J.L., Sickles E.A., Yaffe M.J., and Logan-Young W.W. *A Guide to Mammography and Other Breast Imaging Procedures*. Technical Report 149, National Council on Radiation Protection and Measurements. Bethesda, 2004.
- Gonzalez R.C. and Woods R.E. *Digital Image Processing*. Pearson Education, Inc., 3era. edition, 2008.
- Karssemeijer N. and Thijssen M.A. *Determination of contrast-detail curves of mammography systems by automated image analysis*. In K. Doi, M.L. Ginger, R.M. Nishikawa, and R.A. Schmidt, editors, *Digital Mammography*, pages 155–160. Elsevier, 1996.
- Karssemeijer N. and Thijssen M.A. Readout of CDMAM 3.4 images by human observers. 2004.
- Perry N., Broeders M., de Wolf C., Törnberg S., Holland R., and von Karsa L. *European Guidelines for quality assurance in breast cancer screening and diagnosis*. European Communities, European Breast Cancer Network (EBCN) Coordination Office International Agency for Research on Cancer 150 cours Albert-Thomas F-69372 Lyon cedex 08 France, 4ta. edition, 2006.
- Preim B. and Bertz D. *Visualization in Medicine: Theory, algorithms, and applications*. Morgan Kaufmann Publishers, 2007.
- Shih F.Y. *IMAGE PROCESSING and MATHEMATICAL MORPHOLOGY: Fundamentals and Applications*. CRC Press Taylor & Francis Group, 2009.
- Siemens A. G. Uptime services. 2008.
- Verbrugge B. *VALIDATION OF ANALYSIS METHODS FOR AUTOMATED CDMAM READING*. Master's Thesis, Katholieke Universiteit Leuven, 2007.
- Visser R. and Karssemeijer N. *Manual CDCOM version 1.5.2: software for automated readout of CDMAM 3.4 images*, 2008.